Available on CMS information server

CMS NOTE 2002/049

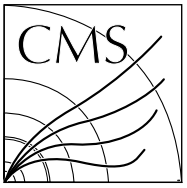

The Compact Muon Solenoid Experiment

CMS Note

Mailing address: CMS CERN, CH-1211 GENEVA 23, Switzerland

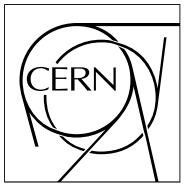

11 November 2002

Position Determination of the Pixel Hits

S. Cucciarelli

University of Basel, Switzerland

D. Kotlińsky

Paul Scherrer Institute, Switzerland

T. Todorov

IN2P3, Strasbourg, France

Abstract

This Note presents a description of the algorithms used to determine the position of pixel hits and its error. Two estimators of the position and error of the pixel clusters have been developed. Each two estimator can be used at a different step of the track reconstruction. One can be applied initially, at the track seeding stage. The other can be used when the approximate trajectory is known. The studies of the spatial resolution of pixel hits as a function of the track impact angles are also described.

1 Introduction

This Note presents a description of the algorithms used to evaluate the positions of the pixel hits and their errors. Two estimators of the cluster parameters have been implemented, a precise one and a less precise but faster (standalone) estimator. The precise estimator uses also the track information. Depending on the stage of the track reconstruction one can use the precise or the standalone cluster parameter estimator. The precise estimator can be used not only when tracks are reconstructed in the whole CMS Tracker, but also when tracks are partially reconstructed (if at least three hits are connected, a track candidate is available). Both the estimators have been implemented in the reconstruction software for CMS analysis [1].

An accurate study of the displacement of the measured position from the true position (residuals) of the pixel hits has been performed as a function of several important parameters which will be defined in the following. All the studies presented in this note refer to single muon events with 100 GeV transverse energy.

2 Pixel Detector Simulation

The CMS Tracker consists of the Pixel detector and the Silicon Strip detector. The Pixel layout considered in the simulation consists of three barrel layers with two endcap disks on each side. The three barrel layers will be located at mean radii 4.4, 7.3 and 15 cm and will be 53 cm long. The two disks will be placed on each side at 34.5 and 46.5 cm from the interaction point. To achieve the optimal resolution of the vertex position in both the r-ϕ and the z coordinates, a design with a square pixel shape 150 $\times$ 150 μm^2 and thickness 300 μm^2 is used. The effect of charge sharing induced by the large Lorentz drift in the 4 T magnetic field is also considered. The whole pixel system consists of about 1400 detector modules arranged into half-ladders of 4 identical modules each in the barrel, and blades with 7 different modules each in the disks. The detectors are 20° tilted in the end disks resulting in a turbine-like geometry. A more detailed description of the Pixel layout can be found in Reference[2].

To read out the detector about 16000 readout chips are bump-bonded to the detector modules. The total number of readout channels is about 44 $\times$ 10^6. The default noise used in the simulation is σ = 500 electrons and the readout threshold for a pixel is 5 σ.

3 Cluster Finding and Definitions of Parameters

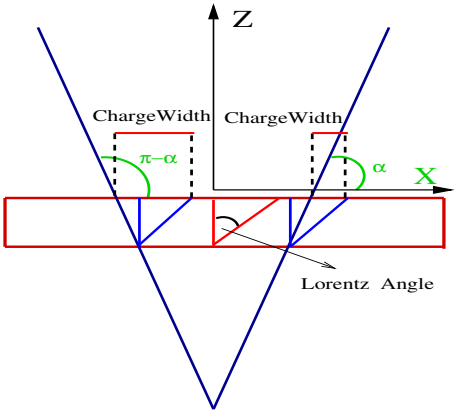

Figure 1: Definition of the track's α impact angle with respect to the detector in the local frame. In the barrel detector, the local x-z plane coincides with the r-ϕ plane of the CMS global reference frame.

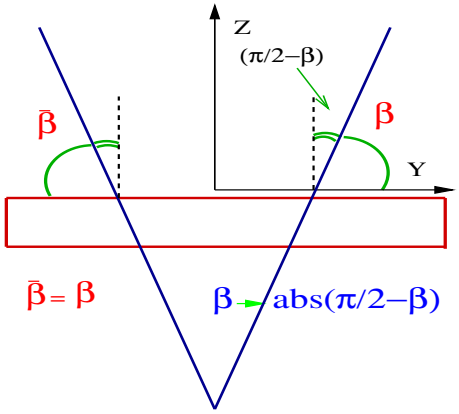

Figure 2: Definition of the track's β impact angle with respect to the detector in the local frame. In the barrel detector, the local y-axis is parallel to the beam and the magnetic field direction. In the endcap disks the magnetic field vector forms an angle of about 20° with the y-axis.

This Section presents a brief description of the cluster finding algorithm and the definition of the most important parameters used to estimate the position and the error of the pixel hits.

Pixels above threshold are analyzed by a cluster finding algorithm. A cluster is defined as a set of adjacent pixels.

The cluster finding algorithm starts from a pixel with signal to noise greater than 6 and moves around in order to merge near pixels (pixels adjoining a corner are considered adjacent). For each cluster, its size in two direction and its total charge is estimated. The cluster charge is compared with a threshold defined in unit of noise as 10.1 σ.

In order to evaluate the hit position from a given cluster, the impact angle of the track to the detector unit (module) has to be considered. The two projections of the track impact angles, α and β, are defined as sketched in Figures 1 and 2 respectively. They are defined as the projections with respect to the detector unit surface onto the x-z and y-z planes. The coordinate system is the local frame with respect to the detector unit. The z-axis is always perpendicular to the surface of the detector unit. For barrel detectors the local x-axis is on the plane transverse to the beam direction and the local y-axis is parallel to the beam axis, while for endcap detectors, the local x-axis is along the radial direction.

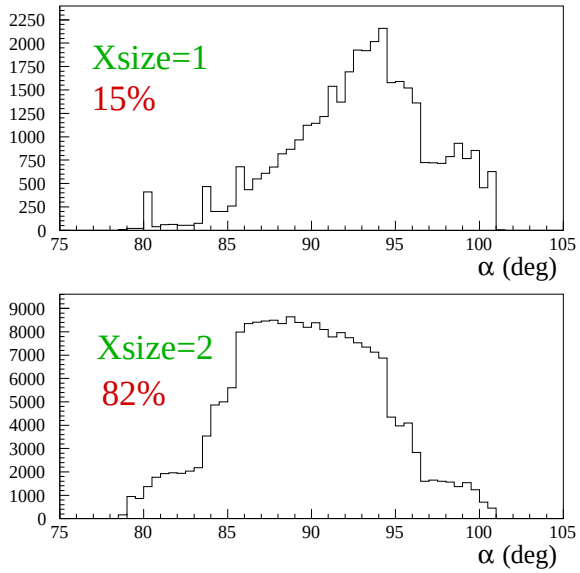

Figure 3: Distributions of the α angle for x cluster size equal 1 (top) and 2 (bottom) for the barrel detector. The fraction of total reconstructed hits in the barrel corresponding to a given cluster size is also shown.

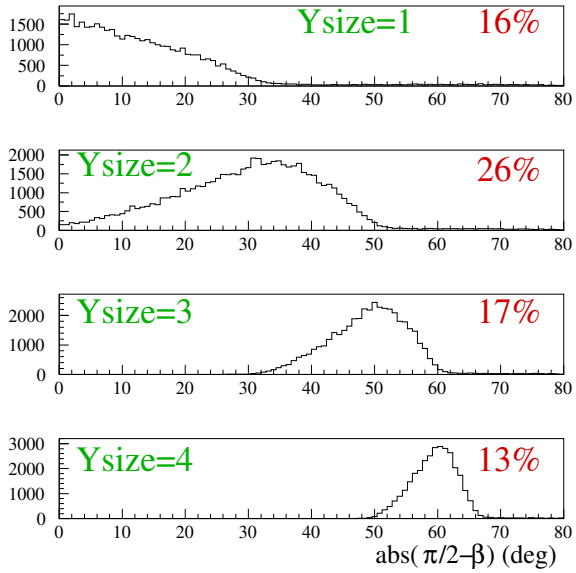

Figure 4: Distributions of the $\mathrm{abs}(\pi/2-\beta)$ angle for y cluster size from 1 (top) to 4 (bottom) for the barrel detector. The fraction of total reconstructed hits in the barrel corresponding to a given cluster size is also shown.

The charge width is the projection on the x, y local directions of the area where the charge is collected on the detector surface. This parameter will be used in the determination of the hit position, as described in Section 4. In the local x-direction, both the geometrical width, due to track inclination, and the Lorentz shift contribute to the charge width calculation. In terms of the impact angle, the charge width in x and y direction is defined as

$$\begin{aligned} \mathrm{W}_x &= \mathrm{LorentzShift} + \mathrm{T}\cdot\tan(\pi/2-\alpha), \\ \mathrm{W}_y &= \mathrm{T}\cdot\tan(\pi/2-\beta); \end{aligned} \tag{1}$$

where T is the detector thickness. For barrel detectors with a thickness of 300 μm, the Lorentz shift is $\sim$156 μm, which is always larger than the geometrical contribution in the local x direction. This leads to an increase of the charge width in the angular region $\alpha < \pi/2$ and a decrease for $\alpha > \pi/2$. There is a Lorentz shift also in the forward detectors, induced by the fact that the detectors are rotated by an angle of 20° around the local x direction. In this way the component of the magnetic field parallel to the local y direction ($\mathrm{B}_0\cdot\sin(20°)$) produces a Lorentz shift in the x direction. This amounts to $\sim$53 μm and it always increases the geometrical width.

When there is no track information, α and β angles are evaluated assuming that the track is coming from the interaction region. For the barrel detectors they are obtained as

$$\tan(\pi/2-\alpha) = \frac{x_C - x_0^{Det}}{R^{Det}}, \tag{2}$$

$$\tan(\pi/2-\beta) = \frac{Z^{Det} + (y_C - y_0^{Det})}{R^{Det}}; \tag{3}$$

where (x_C, y_C) are the local coordinates of the geometrical center of the cluster, (x_0^{Det}, y_0^{Det}) is the middle of the detector in the local frame and R^{Det} and Z^{Det} are the radial and longitudinal detector's coordinates in the global frame. For endcaps, the detector polar angle is used as $(\pi/2 - \alpha)$, while $(\pi/2 - \beta)$ is fixed by the tilt angle value of 20°.

Figure 3 shows the α distributions for cluster size x-size=1, 2 in the barrel x direction. The α distribution for cluster size 1 is shifted to the high α values corresponding to the smallest charge width, on the other hand for cluster size 2 the α distribution shows the highest statistic for the lowest α values. The three steps in the α distribution for cluster size 2 correspond to the three pixel layers in the barrel.

Figure 4 shows the distribution of $\mathrm{abs}(\pi/2 - \beta)$ for pixel hits in the barrel. Since there is no Lorentz angle in y direction, the resolution behavior is symmetrical with respect to β and $(\beta - \pi/2)$, thus always $\mathrm{abs}(\pi/2 - \beta)$ will be considered as the impact angle. In the y direction the cluster size can be greater than 2 and the β range depends on the cluster size.

4 Determination of the Hit Position

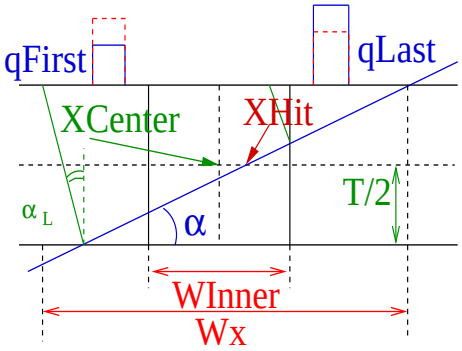

Figure 5: The method used to calculate the local x position of pixel hits in terms of the width W_x and the edge charge of the cluster is sketched. The Lorentz angle α_L induces a shift on the charge width.

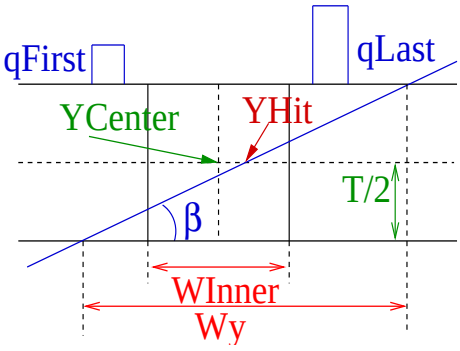

Figure 6: The method used to calculate the local y position of pixel hits in terms of the width W_y and the edge charge of the cluster is sketched.

The position of pixel hits is estimated independently in both x and y local directions. If only one pixel has been hit, the position coordinate is the middle of the pixel. For bigger clusters the position is moved with respect to the center of the cluster by a quantity which depends on the edge charge of clusters and the charge width, W_x and W_y. The precise position estimator is based on the charge width defined in Equation 1 with α and β angles coming from the track. The standalone position estimator uses the evaluation of the track impact angles in Equations 2 and 3 in order to calculate the charge width. To minimize charge fluctuations, only the charge deposited in the first and last row (column) are used to compute the x (y) coordinate and the charge distribution in the inner pixels is supposed to be flat. Accordingly, only the length of the charge width in the first and last pixels of the cluster is considered in the position estimator.

Figures 5 and 6 show how the displacement of the hit position from the center of the cluster is calculated. For the local x coordinate the hit position is computed as

$$x_{hit} = x_C + \frac{q^{row}_{Last} - q^{row}_{First}}{2(q^{row}_{Last} + q^{row}_{First})}|W_x - W^x_{Inner}| - \frac{1}{2}\mathrm{LorentzShift}; \quad (4)$$

where x_C is the geometrical center of the cluster, q^{row}_{First} and q^{row}_{Last} are the charges deposited in the first and last row respectively and W^x_{Inner} is the length along the x-axis of the inner pixels covered by the cluster, defined as (x-size-2)$\times$pitch for cluster size larger than 2 and zero otherwise. Since the local frame is defined in the innermost region of the detector unit, one needs to project the measured position into the inner plane by subtracting half a Lorentz shift. When the charge width W_x is greater than the cluster size or W^x_{Inner} greater than W_x, only the charge information is retained and Equation 4 is used with the constraint: if $|W_x - W^x_{Inner}| > 2$, then $|W_x - W^x_{Inner}| \equiv 1$. The contribution from the Lorentz angle is included in the charge width definition. This algorithm is used by both the precise and the standalone x position estimator when the x-cluster size is larger than 1. In fact, the prediction

of the impact angle on the transverse plane is precise enough even if no track information is available, due to the small smearing of the primary vertex on the transverse plane ($\sim$15 μm).

For the y coordinate the precise position estimator uses a formula equivalent to Equation 4 for any y cluster size larger than 1:

$$y_{hit} = y_C + \frac{q^{col}_{Last} - q^{col}_{First}}{2(q^{col}_{Last} + q^{col}_{First})}|W_y - W^y_{Inner}|; \quad (5)$$

where y_C is the geometrical center of the cluster, q^{col}_{First} and q^{col}_{Last} are the charges deposited in the first and the last column respectively and W^y_{Inner} is the length along the y-axis of the inner pixels hit, (y-size-2)$\times$pitch for cluster size larger than 2 and zero otherwise. Similarly to the x position computation, $|W_y - W^y_{Inner}|$ is set to 1 if $|W_y|$ is larger than the y size of the cluster. The knowledge of the track angle allows a precise evaluation of the charge width also for very long clusters. When the track angle is not available (standalone estimator) Equation 5 is used only for y-cluster size smaller than 4 with the constraint $|W_y - W^y_{Inner}| = 1$ if $|W_y - W^y_{Inner}| > 1$. For very long cluster sizes charge fluctuations spoil the resolution of this method and the $edge$ algorithm is used instead. This is equivalent to the formula in Equation 5 with $|W_y - W^y_{Inner}| = 1$.

To further improve the resolution of the precise position estimator, a correction (η-correction) is introduced to minimize the bias on the measured hit position in the α and $\mathrm{abs}(\pi/2 - \beta)$ bins where the charge width is largest. The bias on the position is shown in Figure 7 and Figure 8 for the x and y coordinate respectively. These plots represent the average value of the residual distribution as a function of the charge ratio $q_{First}/(q_{Last} + q_{First})$ without and with the η-corrections, the different curves correspond to different bins of the track impact angles. The displacement from zero of these curves quantifies the bias on the position. As can be seen, the largest effect appears for values of the impact angle corresponding to the largest charge width. In this case, in addition to the charge fluctuations effects, there is a substantial probability for the cluster to be longer than the effective size. After this effect has been corrected by an analytical function, the discrepancy from zero of the average value of the residuals is less than 3 μm. For the x-coordinate, the same η-corrections are applied in both the precise and standalone position estimators, due to the fact that in the transverse plane α is precisely evaluated also from the detector position.

In Figure 9, x resolutions for cluster size 2 and y resolutions for cluster sizes 2 and 3 are shown as a function of the charge width. As can be seen, the algorithm gives exactly the same performance in the two dimensions where the ranges of W_x and W_y overlap.

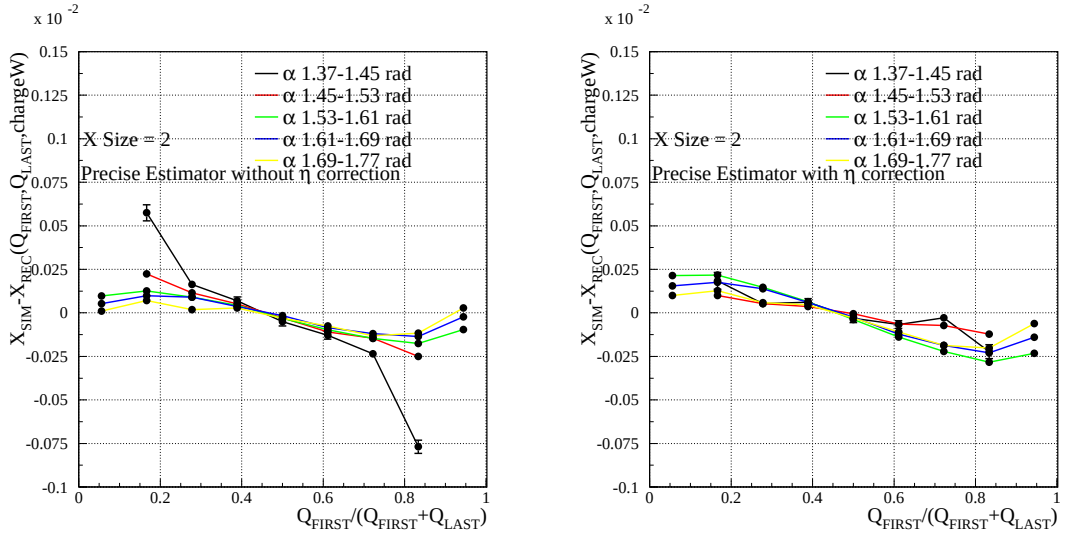

Figure 7: The average value of the x-residual as a function of the charge ratio $q^{row}_{First}/(q^{row}_{First} + q^{row}_{Last})$ for x-cluster size 2 without any η-correction (on the left) and with η-correction (on the right). The different curves correspond to different α bins.

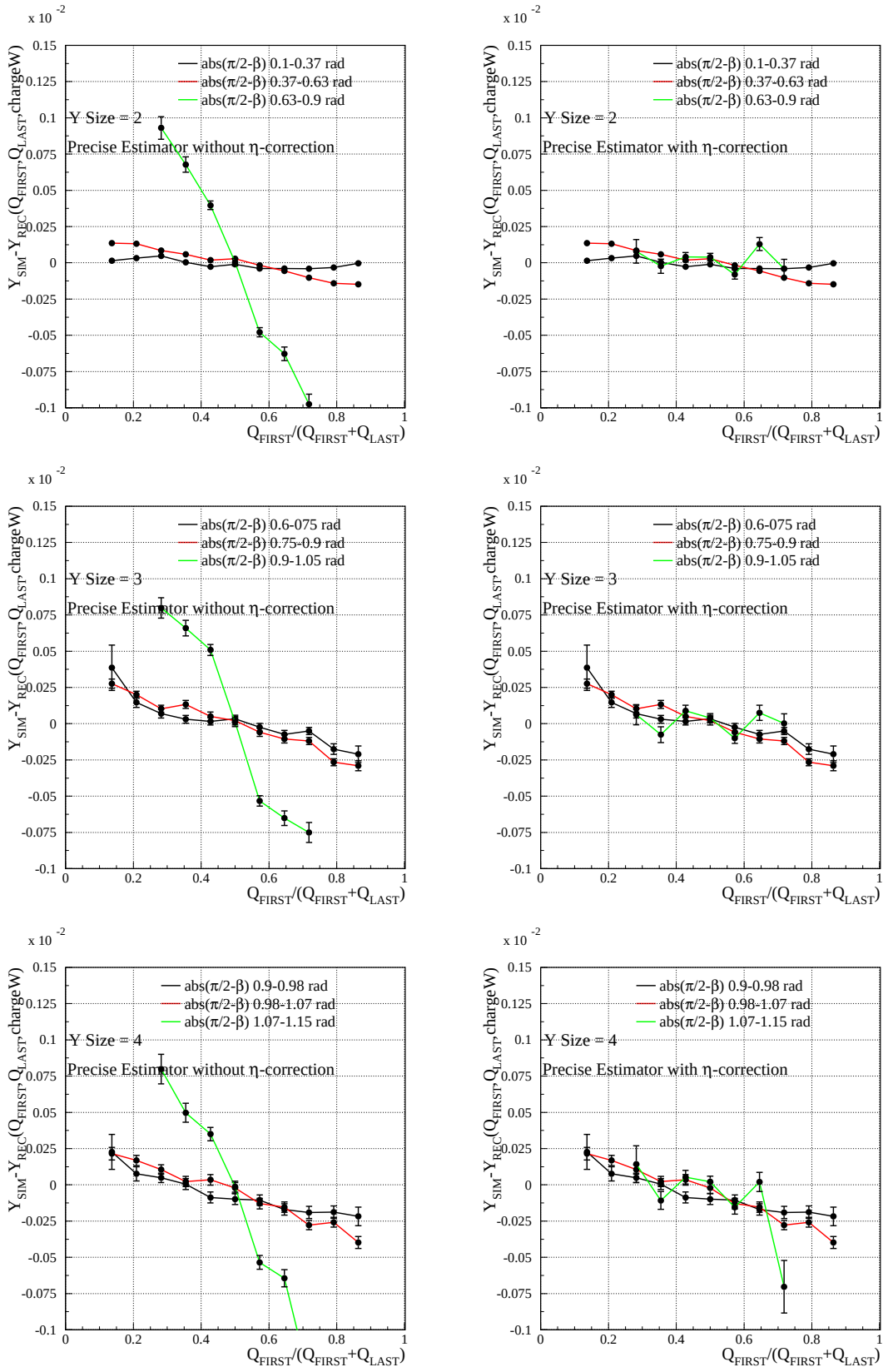

Figure 8: The average value of the y-residual as a function of the charge ratio $q^{col}_{First}/(q^{col}_{First} + q^{col}_{Last})$, from the top to the bottom for y-cluster size 2, 3 and 4. The plots on the left are without any η-correction and on the right with η-correction. The different curves in the pictures correspond to different $\mathrm{abs}(\pi/2 - \beta)$ bins.

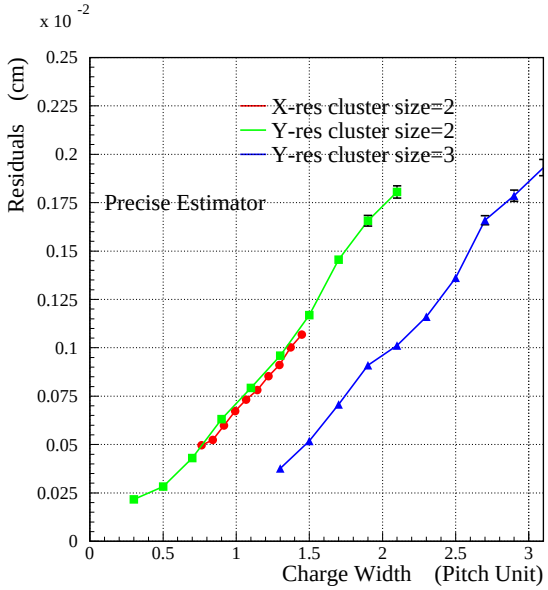

Figure 9: Pixel resolutions, in the x direction for x-cluster size 2 and in the y direction for y-cluster size 2 and 3, as a function of the charge width.

5 Error Treatment

The hit resolution depends on several factors, directly connected to the pixel detector, like the pixel size and thickness, and to the reconstruction, like the clustering algorithm, pixel thresholds and the track impact angles. As for the position estimation, the error determination is made independently in the x and y coordinates.

Two different estimations of the errors have been studied: a "precise error estimator" and a "standalone error estimator". The first one relies on the knowledge of the track impact angle from either a partial or complete track reconstruction, evaluating the error as a function of the track angles α and β for each value of the cluster size. On the other hand, the standalone error estimator in the barrel uses the r.m.s values of the reconstructed hit residuals, separately for each cluster size, and in the endcap uses a simple linear parametrization of the residual r.m.s. with respect to the detector polar angle.

The precise error estimation uses the knowledge of the track impact angle. The spatial resolution in the x direction mostly depends on α and in y direction mostly depends on $|\pi/2 - \beta|$. For the barrel hits, the x resolution depends also on the projection of the track angle into the $y - z$ plane. Similarly, the y resolution depends also on the impact angle in the $x - z$ plane. For this reason, the parametrization of the error is made as a function of three parameters, the cluster size in x or y direction and the two angles α and $|\pi/2 - \beta|$. For the endcaps, only the cluster size in x (y) direction and the α ($|\pi/2 - \beta|$) angle are considered.

In order to perform a three-dimensional parametrization of the error, a kind of "matrix" has been implemented, looking at the behavior of the residuals of the reconstructed hit with respect to the simulated one, for the different cluster topologies and in different α and $|\pi/2 - \beta|$ bins. For the x (y) direction, each element of this matrix contains a mono-dimensional error parametrization as a function of the α ($|\pi/2 - \beta|$) angle. Two indices identify this element, the first one refers to the cluster size and the second one identifies the bin of the $|\pi/2 - \beta|$ (α) angle where the mono-dimensional parametrization is valid. Depending on the behavior of the resolution, the mono-dimensional error parametrization could be either a polynomial fit or a linear interpolation. In according with this, each element of the matrix consists of a vector containing either the fit parameters, when a polynomial function is used to parametrize the error, or the resolutions points, when the error is evaluated with a linear interpolation between the two closest resolution points.

If the track angle is not available the standalone error estimator is used. For the barrel, the error depends only in the cluster size. For the endcaps, the error is parametrized with a linear function of the polar angle of the detector unit.

For clusters found at the edge of a detector unit, the maximum error is given as the pitch over $\sqrt{12}$, in both the precise and the standalone estimators.

	y Barrel Resolutions (μm)				x Barrel Resolutions (μm)	
Cluster Size	1	2	3	4	1	2
Layer 1	30.3 ± 0.2	10.2 ± 0.1	13.0 ± 0.1	14.2 ± 0.2	15.7 ± 0.1	11.1 ± 0.04
Layer 2	30.4 ± 0.1	10.2 ± 0.1	13.1 ± 0.1	14.1 ± 0.2	12.7 ± 0.1	9.5 ± 0.1
Layer 3	30.0 ± 0.1	9.8 ± 0.1	12.7 ± 0.1	14.0 ± 0.2	11.8 ± 0.1	9.0 ± 0.04
	y Forward				x Forward	
Disk 1	22.2 ± 0.1	6.4 ± 0.06			17.8 ± 0.1	11.8 ± 0.07
Disk 2	22.0 ± 0.1	6.5 ± 0.06			18.1 ± 0.1	12.3 ± 0.1

Table 1: Spatial resolution of pixel hits for different cluster sizes, for the three barrel layers and the two forward disks. The resolution values and errors are obtained from the Gaussian width of the fit of residuals and its error.

The error evaluation does not explicitly depend on the pixel layer where the hit is collected. The average spatial resolution for each layer in the barrel and forward pixel detector are listed in Table 1 for different cluster sizes. The resolution values listed in the table are the width of a Gaussian fit to the residual distribution of the reconstructed hits. As can be seen, for a given cluster size the pixel resolution is almost the same for every barrel layer or forward disk except in the transverse plane. There is a slight degradation of the resolution by increasing the detector radius, due to fact that the α range becomes smaller and less charge is collected on average into a pixel.

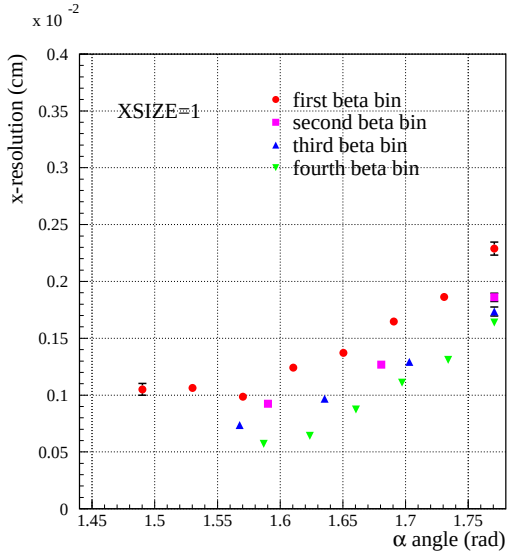

Figure 10: Spatial resolution in the x direction for barrel detectors, for cluster size 1, as a function of α. The different markers correspond to different $|\beta - \pi/2|$ bin on the range from 0 to 1.4 Radians.

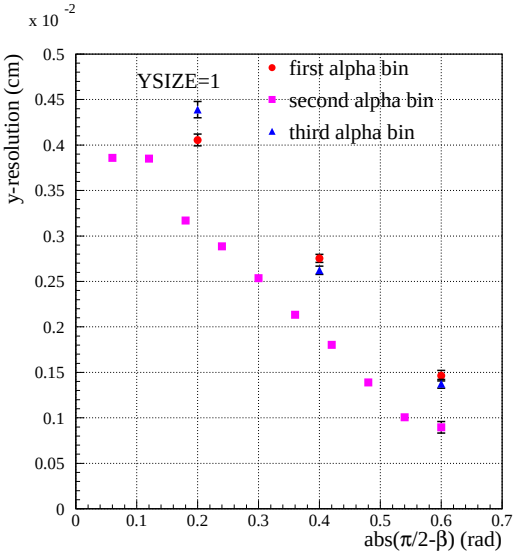

Figure 11: Spatial resolution in the y direction for barrel detectors, for cluster size 1 as a function of $|\beta - \pi/2|$. The different markers correspond to different α bin on the range from 1.37 to 1.77 Radians.

In order to look in more detail at the barrel spatial resolution, the width of the residuals is shown for each cluster size and for each angle bin considered on the precise error estimator. Figure 10 shows the behavior of the x-spatial resolution for cluster size 1. The degradation of the resolution is due to the fact that less charge is collected on the pixel surface for high α value. Similarly the y resolution for cluster size 1 in Figure 11 improves moving to higher β values.

Figure 12 shows the comparison between the standalone and the precise cluster parameter estimator in the case of the x resolution for cluster size 2. There are no significant effects because the α evaluation is precise enough even without track information. On the other hand, a large improvement is evident in Figure 13 in the y-resolution for clusters larger than 1. In this case the hypothesis that the track is coming from (0,0,0) leads to a poor measurement of β due to the uncertainty in the global z coordinate of the primary vertex ($O(\mathrm{cm})$). The knowledge of the β angle strongly improves the estimation of the charge width and consequently of the hit position. The improvement obtained with the precise estimator is shown in Figure 13, where the resolution in y direction is presented as a

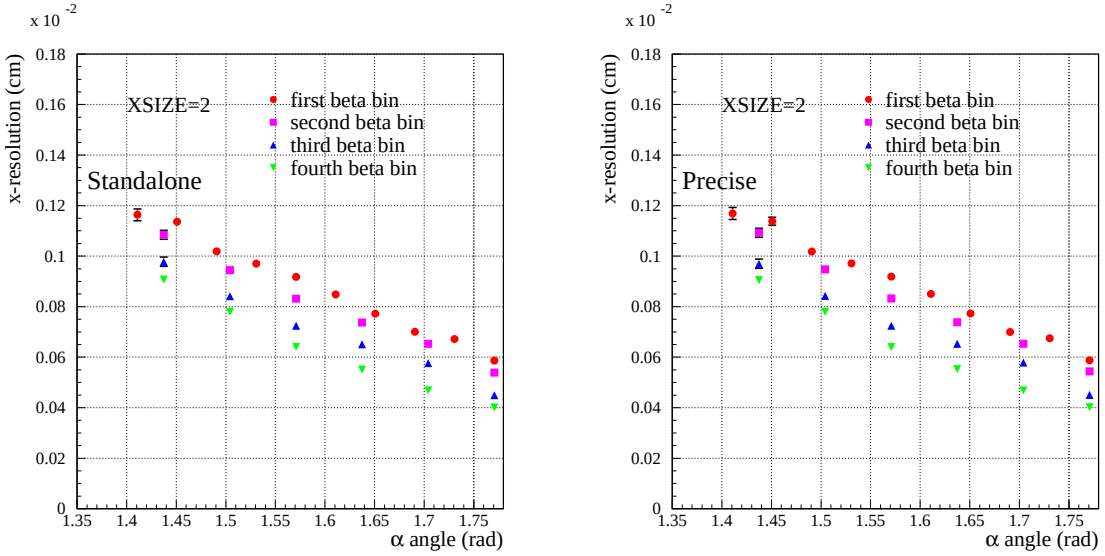

Figure 12: Comparison between the barrel x resolution obtained with the standalone (on the left) and the precise (on the right) cluster parameter estimators, for x cluster size 2. The resolution are shown as a function of the α angle, the different markers correspond to a different $|\beta - \pi/2|$ bins on the range from 0 to 1.4 Radians.

function of $|\beta - \pi/2|$ for different cluster lengths. For cluster larger than 3 the resolution behavior is independent of α, thus only the β parametrization is considered.

The spatial resolution for the forward pixel detectors is shown in Figures 14 to 17. The size of clusters in the forward detectors is 1 with a probability of 30% and 46%, and it is 2 with a probability of 69% and 54%, for the x and y directions respectively. For forward clusters with a given size, the error parametrization is made as a function of $|\alpha - \pi/2|$ or $|\beta - \pi/2|$ for x and y local coordinate respectively. The precise estimator mostly improves the resolution in the y forward direction for cluster size 2 as it is shown in Figure 17.

The results of the error studies presented in this note are summarized in Figures 18 to 22, where the width of the residual pull[1)] distributions are shown as a function of α for x and β for y coordinate and in each bin considered for the precise error estimation. When the standalone estimator is used the error is a constant value for a given cluster size except for the forward x coordinate where a linear parametrization is made as a function of the polar angle of the detector. Thus behavior of the pulls as a function of the impact angles reproduces the resolution behavior. On the other hand, the precise estimator gives a correct good interpretation of errors and the pulls are quite flat around 1.

6 Conclusions

A detailed study of the spatial resolution of pixel hits leads to the implementation of two estimators of the position and error, both of them using the impact angles in order to evaluate the cluster parameters. The precise estimator benefits from the track candidate associated to the hit and the standalone one relies on an estimation of the track angles in terms of the detector's angles. The precise cluster parameter estimator strongly improves the position on y direction and on the forward detectors. The two parameter estimators give almost the same performance on the barrel x position, where the impact angle can be precisely computed independent of the track.

The best x resolution is around 4 μm obtained at the highest value of α, for cluster size 2 and in the barrel. The improvement is most evident in the y position, in particular for low values of $|\beta - \pi/2|$. The largest effect is for y cluster size 2, and the residuals are up to 20 times better than the standalone position estimator. The best resolution in y position is around 3 μm, which is obtained for cluster size 2 and in the barrel detectors. The contribution to the errors coming from the alignment is around 10 μm and it exceeds the spatial resolutions obtained with the precise estimator for a large range of the parameters.

Since the spatial resolution significantly depends on the track impact angle, this knowledge is helpful not only for

[1)] The pull is defined as the ratio of the residual over its error.

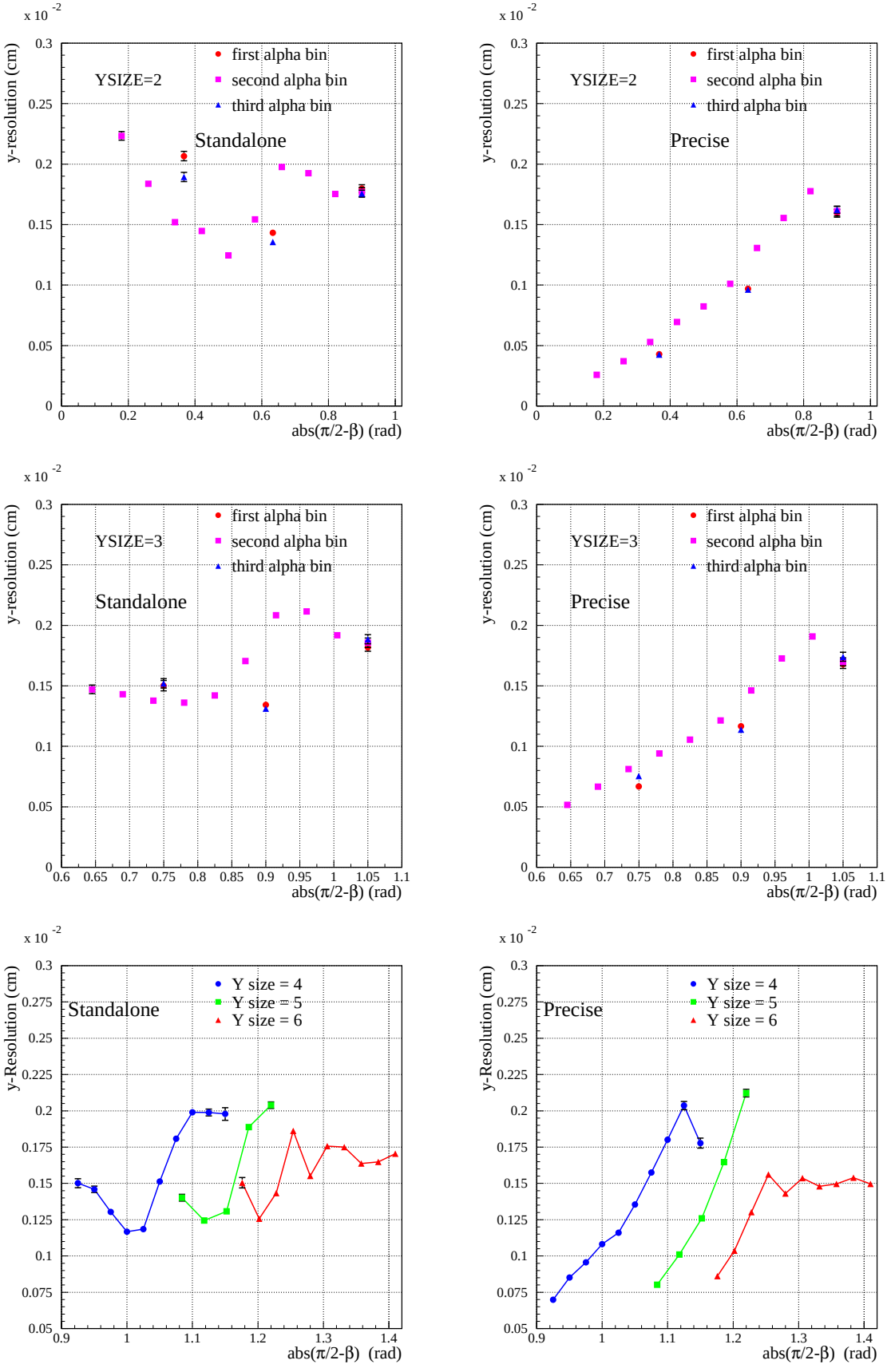

Figure 13: Comparison between the barrel y resolution obtained with the standalone (on the left) and the precise (on the right) cluster parameter estimators, for y cluster size from 2 (top) to 6 (bottom). The resolution are shown as a function of the $\mathrm{abs}(\beta - \pi/2)$ angle, the different markers correspond to a different α bins on the range from 1.37 to 1.77 Radians.

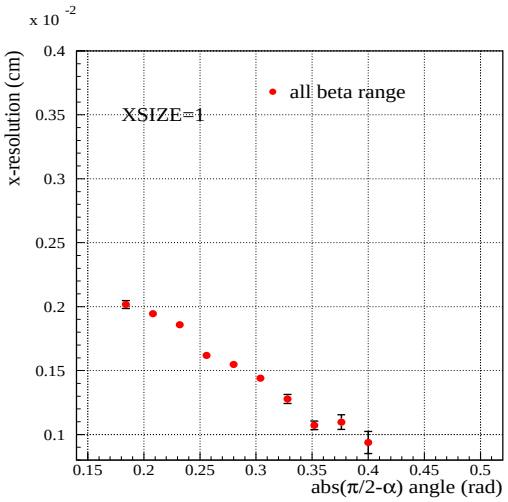

Figure 14: Spatial resolution in the x direction for forward detectors, for cluster size 1, as a function of $\mathrm{abs}(\alpha - \pi/2)$.

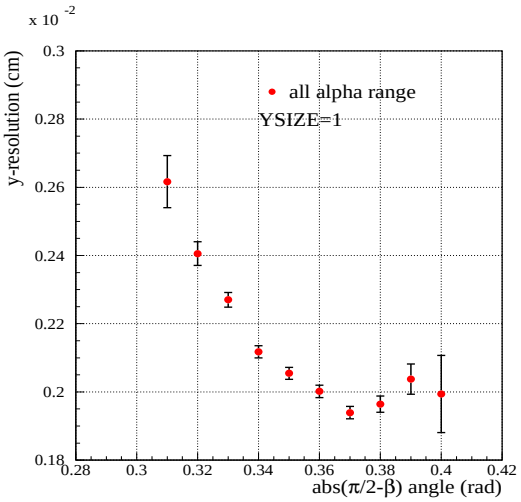

Figure 15: Spatial resolution in the y direction of forward detectors, for cluster size 1, as a function of $\mathrm{abs}(\beta - \pi/2)$.

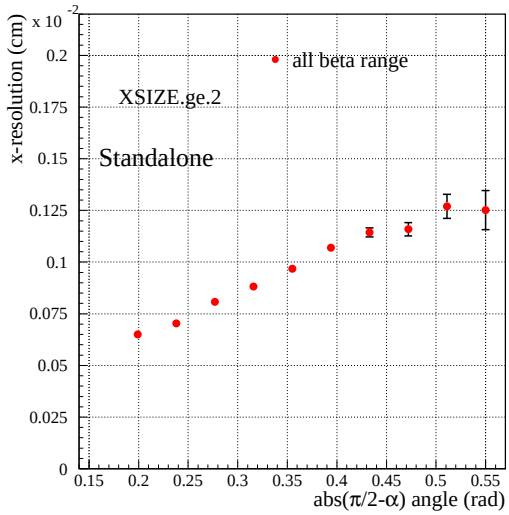

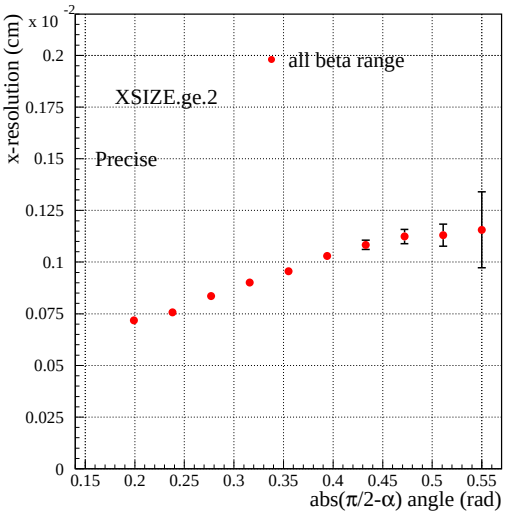

Figure 16: Comparison between the forward x resolution obtained with the standalone (on the left) and the precise cluster parameter estimators (on the right), for x cluster size 2. The resolution are shown as a function of the $\mathrm{abs}(\alpha - \pi/2)$ angle, the different markers correspond to a different $\mathrm{abs}(\beta - \pi/2)$ bins on the range from 0.3 to 0.4 Radians.

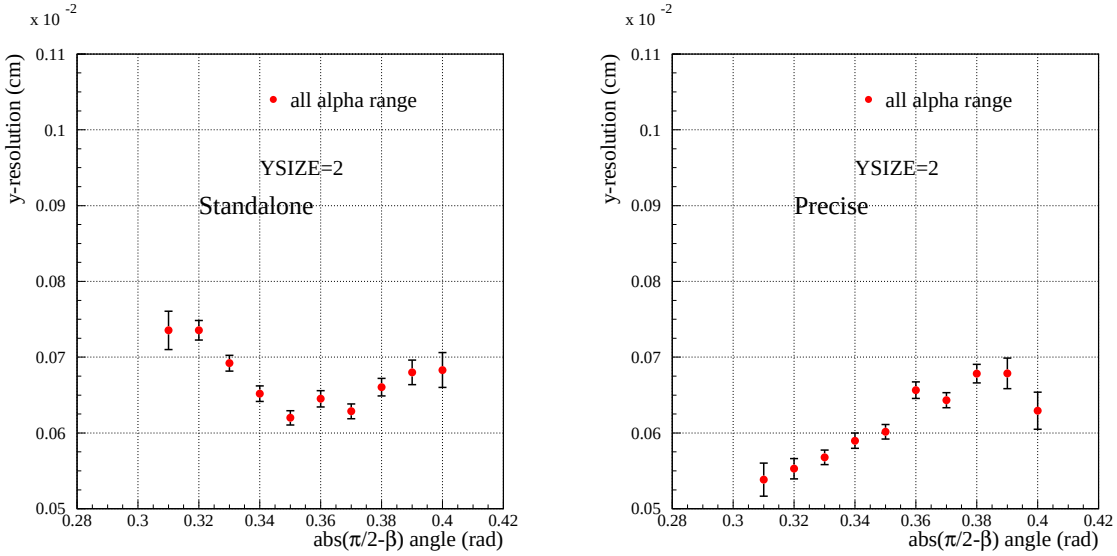

Figure 17: Comparison between the forward y resolution obtained with the standalone (on the left) and the precise (on the right) cluster parameter estimators, for y cluster size 2. The resolution are shown as a function of the $\mathrm{abs}(\beta - \pi/2)$ angle.

a more precise position estimation, but also to give a better error estimation. Of course the behavior of the spatial resolution as a function of the given parameters depends not only on the cluster finding algorithm but also on the particular digitization method used for the detector simulation. Thus the error parametrization needs to be redone in case of a change in the cluster finding and digitization method. All the necessary tools are provided.

These cluster parameter estimators should be tested with real data, by comparing the reconstructed hit position with the hit position extrapolated from the neighboring detectors.

References

[1] **CMS Internal Note 1999/01**, The CMS Software and Computing Group, *"Object Oriented Reconstruction for CMS Analysis"*
(see http://cmsdoc.cern.ch/orca).

[2] **CERN/LHCC 1998/06**, The CMS Collaboration, *"CMS Tracker Technical Design Report"*.

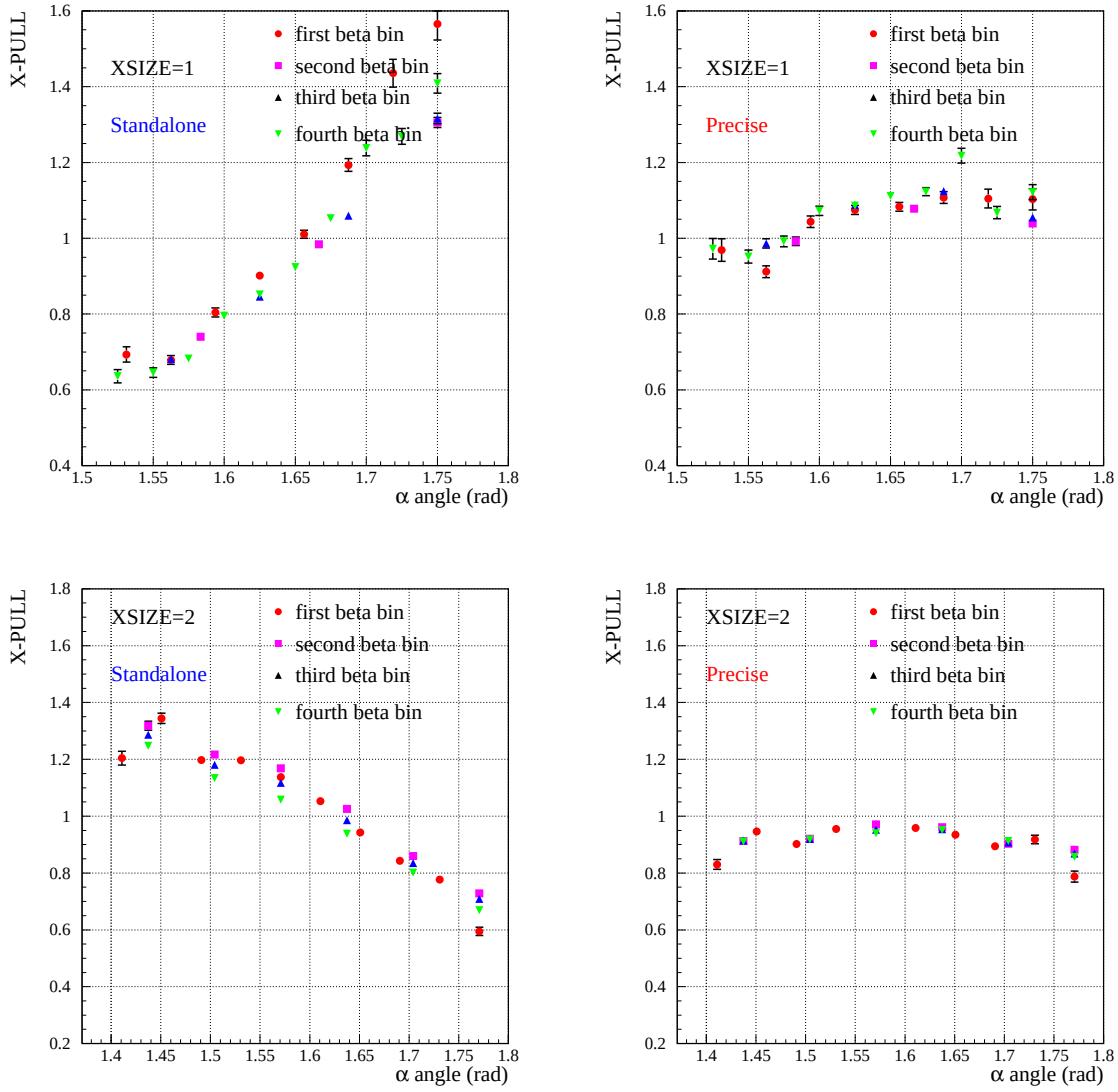

Figure 18: Comparison between the pull of x barrel residuals obtained with the standalone (on the left) and the precise (on the right) cluster parameter estimators, for x cluster size 1 (top) and 2 (bottom). The pulls are shown as a function of the α angle and the different markers correspond to a different $\mathrm{abs}(\beta - \pi/2)$ bins on the range from 0 to 1.4 Radians.

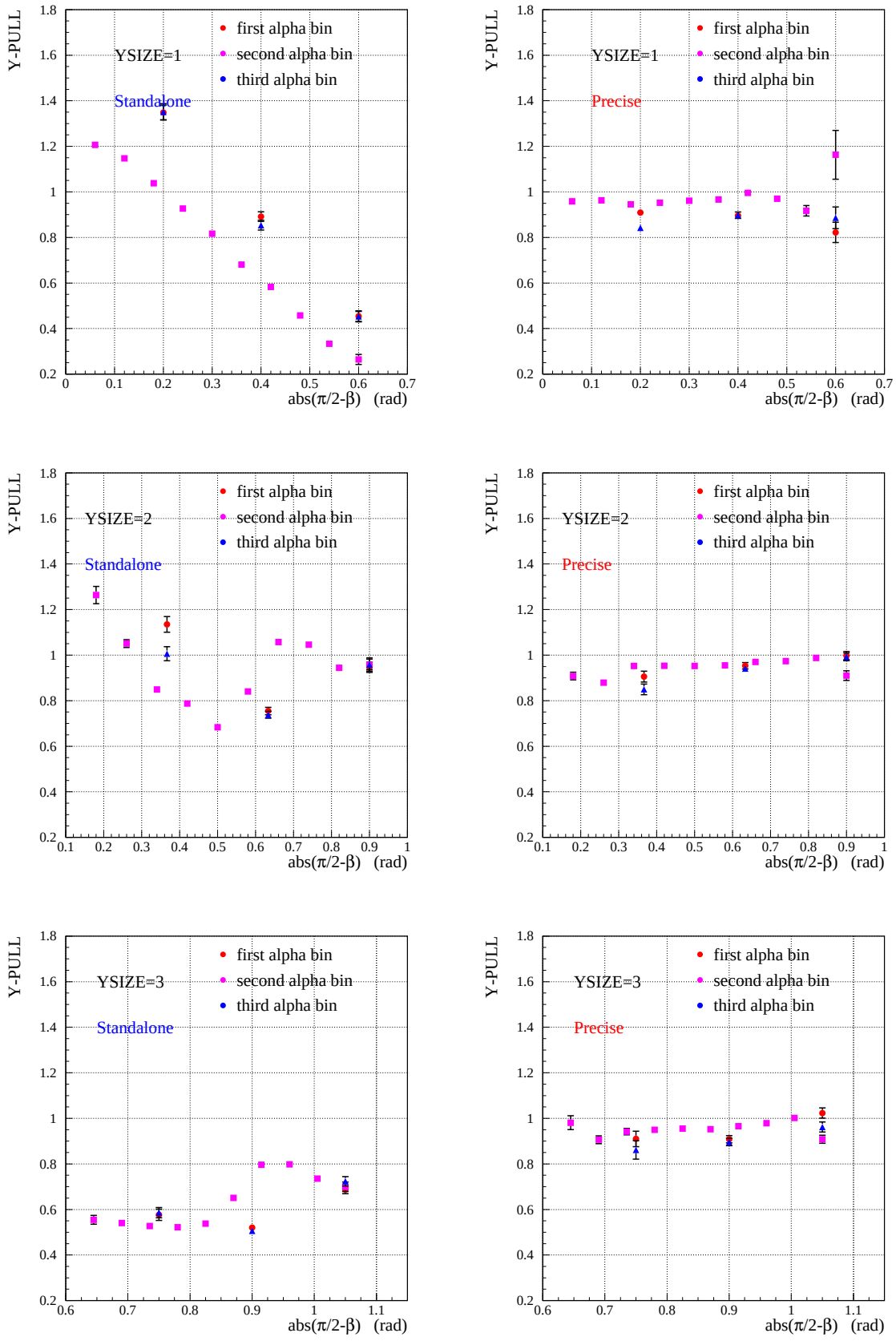

Figure 19: Comparison between the pull of the y barrel residuals obtained with the standalone (on the left) and the precise (on the right) cluster parameter estimators, for y cluster size from 1 (top) to 3 (bottom). The pulls are shown as a function of the $\mathrm{abs}(\beta - \pi/2)$ angle and the different markers correspond to a different α bins on the range from 1.37 to 1.77 Radians.

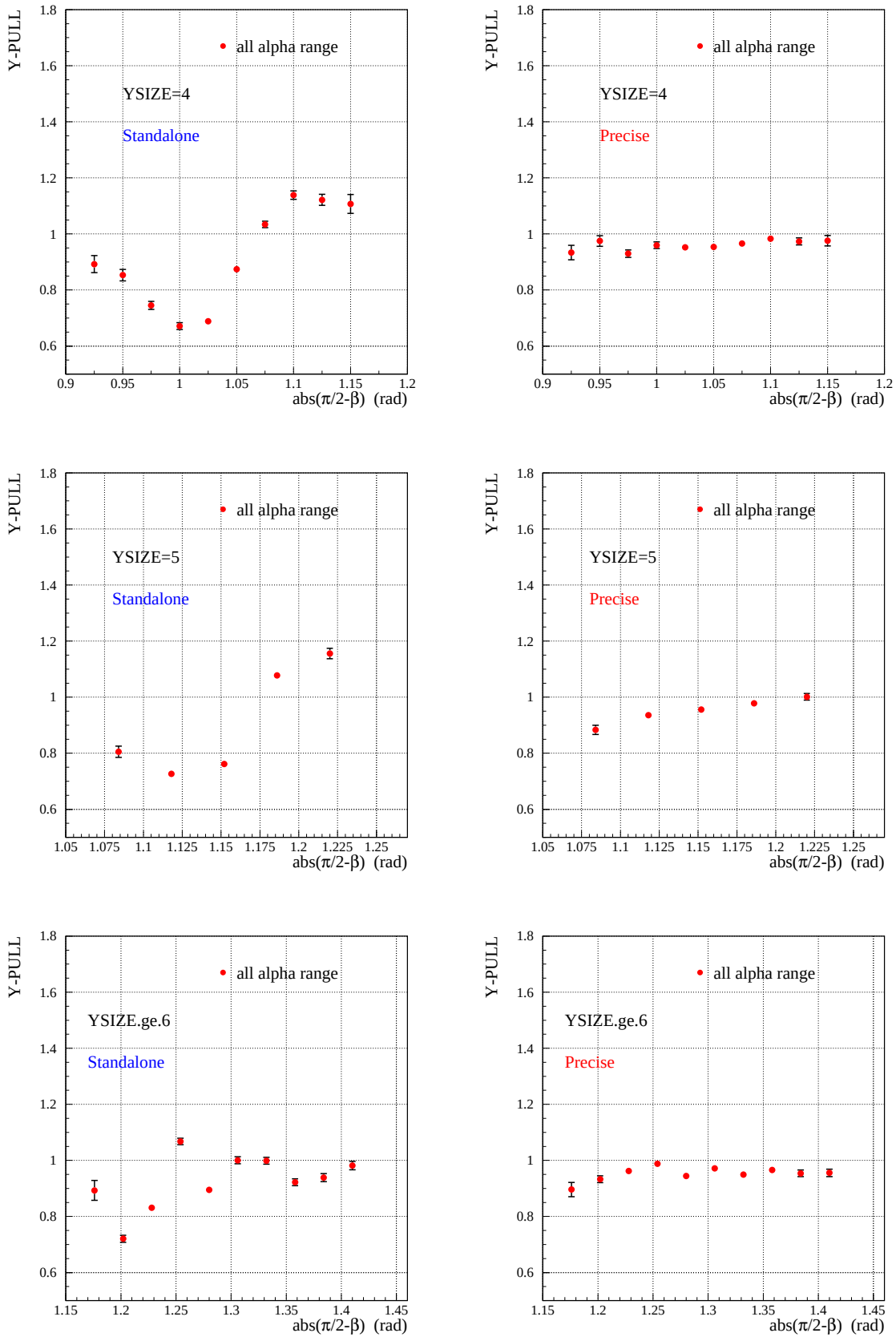

Figure 20: Comparison between the pull of y barrel residuals obtained with the standalone (on the left) and the precise (on the right) cluster parameter estimators, for y cluster size from 4 (top) to 6 (bottom). The pulls are shown as a function of the $\mathrm{abs}(\beta - \pi/2)$ angle and the different markers correspond to a different α bins on the range from 1.37 to 1.77 Radians.

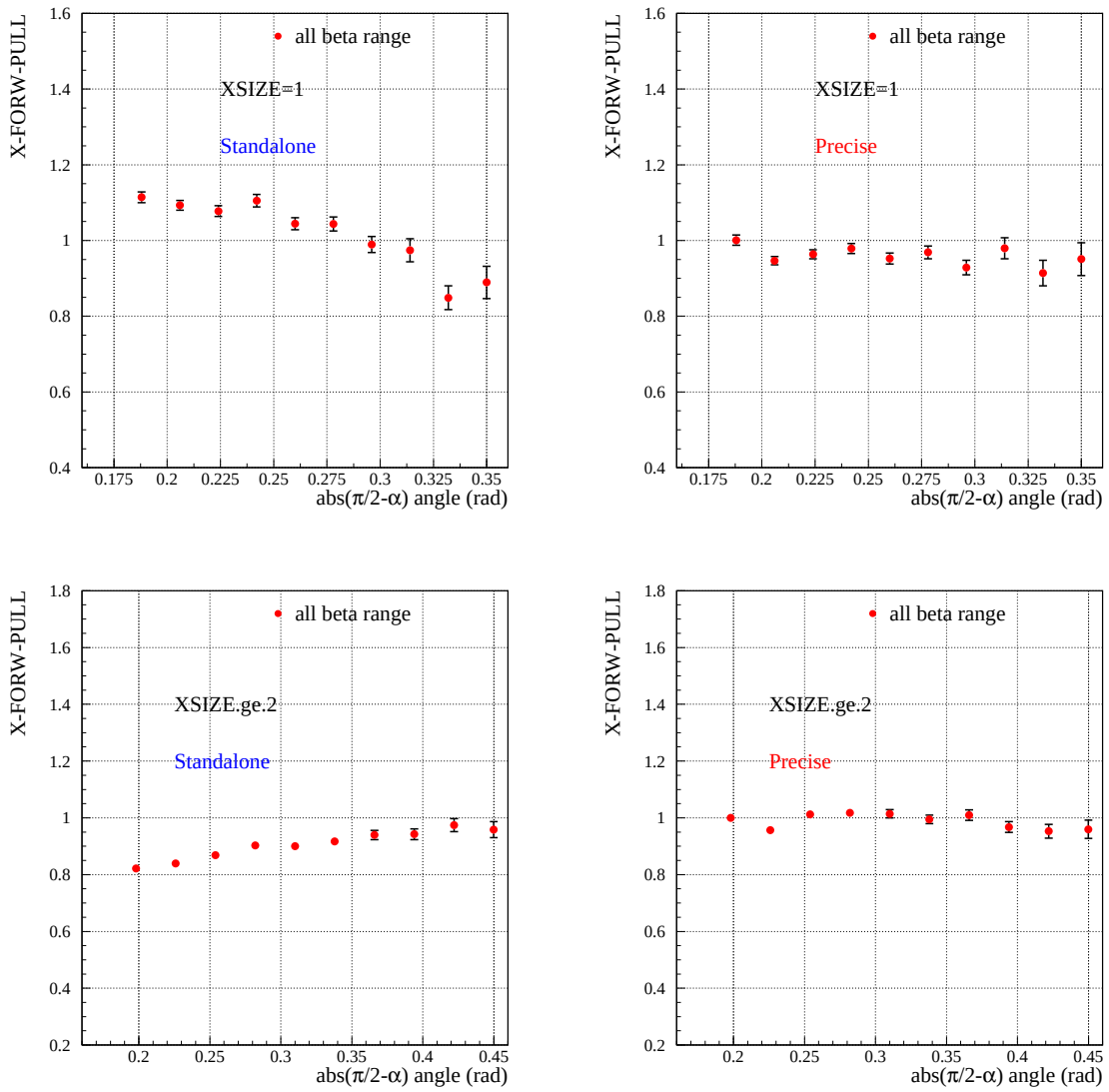

Figure 21: Comparison between the pull of x forward residuals obtained with the standalone (on the left) and the precise (on the right) cluster parameter estimators, for x cluster size 1 (top) and 2 (bottom). The pulls are shown as a function of the $\mathrm{abs}(\alpha - \pi/2)$ angle and the different markers correspond to a different $\mathrm{abs}(\beta - \pi/2)$ bins on the range from 0.3 to 0.4 Radians.

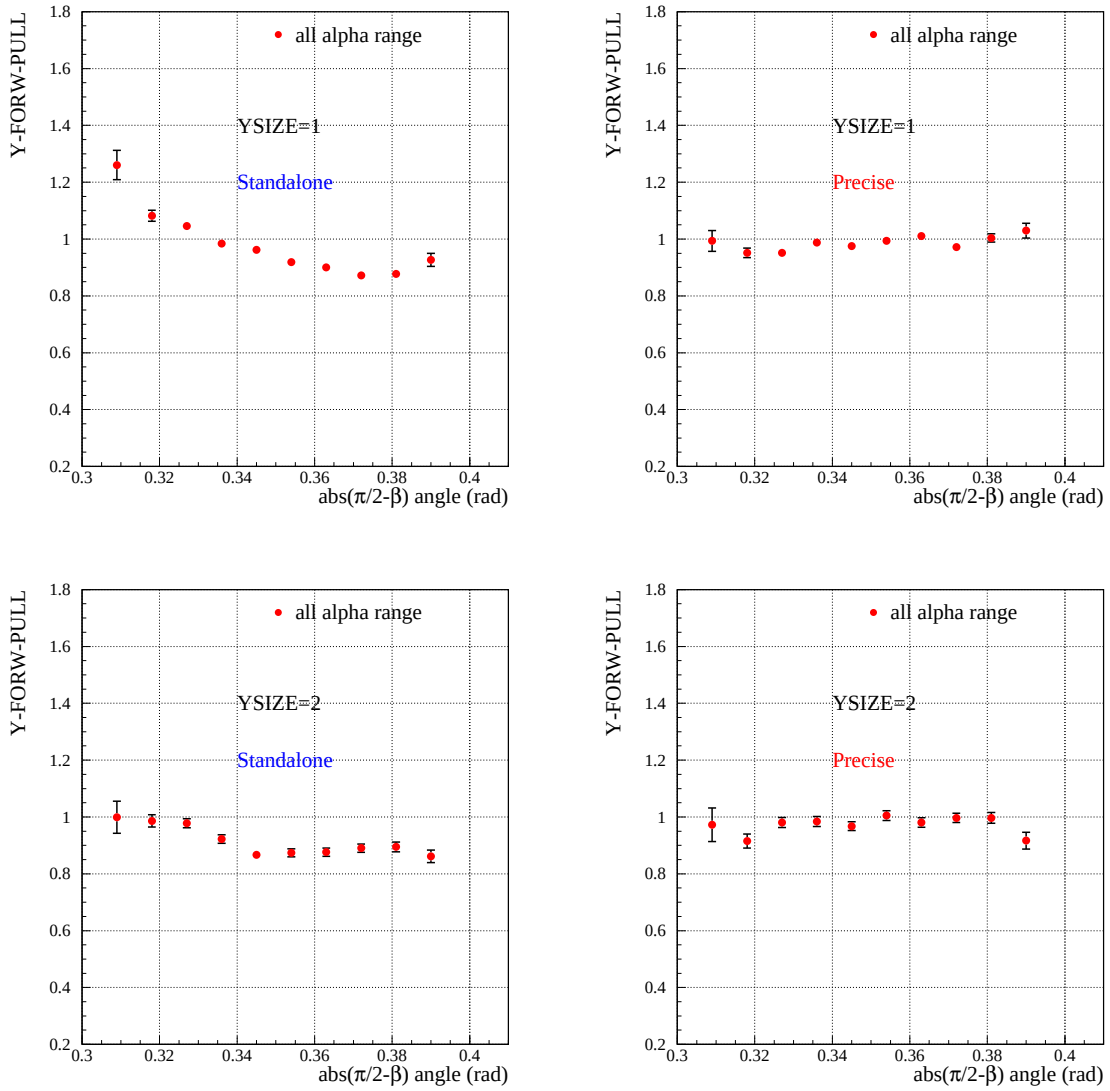

Figure 22: Comparison between the the pull of y forward residuals obtained with the standalone (on the left) and the precise (on the right) cluster parameter estimators, for y cluster size 1 (top) and 2 (bottom). The pulls are shown as a function of the $\mathrm{abs}(\beta - \pi/2)$ angle.